Factor Analysis for Extraction of Blood Time-Activity Curves in Dynamic FDG-PET Studies

Hsiao-Ming Wu, Carl K. Hoh, Yong Choi, Heinrich R. Schelbert, Randall A. Hawkins, Michael E. Phelps and Sung-Cheng Huang

Division of Nuclear Medicine and Biophysics, Department of Molecular and Medical Pharmacology, Laboratory of Structural Biology and Molecular Medicine, UCLA School of Medicine, Los Angeles, California

Arterial sampling in dynamic PET studies can be eliminated by using left ventricular or aortic time-activity curves (TAC) obtained from user drawn regions of interest (ROIs) after appropriate spillover correction. In this study, we evaluated the feasibility of extracting the "pure" arterial TAC from dynamic PET images using factor analysis of dynamic structures (FADS). **Methods:** Computer simulations were used to study the performance of the FADS algorithm with positivity constraints. Ten canine ^{13}N-ammonia and two human FDG-PET dynamic studies were used to extract the blood TACs from FADS. Plasma samples and compartmental model fittings were used to validate the accuracy of the FADS-generated blood factors. **Results:** We found that FADS with positivity constraints was sufficient to extract the blood factor from the composite dynamic images. The "pure" blood-pool TACs that matched well with the arterialized well counter measurements were generated from FADS in the canine and human studies. **Conclusion:** FADS has the potential to accurately extract "pure" blood TAC from dynamic PET images, allowing reliable quantitation of biological information from PET studies without blood sampling, ROI drawing or spillover correction.

Key Words: factor analysis; blood time-activity curve extraction; positron emission tomography; nitrogen-13-ammonia; fluorine-18-fluorodeoxyglucose

J Nucl Med 1995; 36:1714–1722

Functional imaging with PET is a unique tool for investigating normal physiology and pathology in various radiotracer studies. An appropriate compartmental model, in conjunction with a parameter estimation technique, can be used to estimate physiological parameters requiring arterial blood sampling. To avoid such invasive blood sampling, the left ventricular or aortic time-activity curve (TAC) obtained from user-drawn regions of interest (ROIs) has been commonly used. Although ROI methods are convenient, they suffer from accuracy, reliability and reproducibility. In addition, spillover activity from adjacent structures may affect the shape of the blood TAC. For an accurate estimation of parameters in model fittings, a simple but reliable procedure to extract the "pure" blood TAC is advantageous.

Factor analysis of dynamic structures (FADS) has been used to decompose dynamic sequences into component images and their corresponding TACs based on the analysis of the variance in the data (*1–5*). Algorithms have been based on principal component analysis (PCA) followed by oblique rotations with positivity constraints (*1*). In tomographic images such as PET, different anatomical structures do not overlap; partial volume effects and spillover problems, however, may cause activity in the blood pool to be contaminated with activities from the adjacent structures (e.g., myocardium). Therefore, the TAC on a pixel basis (dixel) can be assumed to be a linear combination of activities from different structures. The goal of this study was to explore whether FADS with positivity constraints can separate the component TACs in cardiac PET images. This will allow the pure blood TACs to be extracted from FADS, thereby avoiding conventional ROI drawing and spillover correction.

Phantom simulations and canine ^{13}N-ammonia PET images were used to evaluate the performance of the FADS algorithm. The algorithm was then applied to extract the blood TACs from human FDG-PET images. Plasma samples and compartmental model fittings were used to validate the accuracy of the FADS-generated blood factors.

MATERIALS AND METHODS

FADS Algorithm

The underlying model of FADS hypothesizes that in the image sequences there is a limited number of structures, each of which can be characterized by a specified kinetics or function (*6*). Due to the limitation of scanner resolution, these structures appear to

Received Oct. 17, 1994; revision accepted Feb. 14, 1994.

For correspondence or reprints contact: Carl K. Hoh, MD, Division of Nuclear Medicine and Biophysics, Dept. of Molecular and Medical Pharmacology, UCLA School of Medicine, 10833 Le Conte Ave., Los Angeles, CA 90095-6948.

overlap. Therefore, the signal measured at each dixel (pixel activity as a function of n sample time points) is a weighted sum of the underlying kinetics or functions. This basic hypothesis can be formulated as:

$$Y(p, t) = \sum_{k=1}^{K} (I_k(p) \cdot C_k(t)) \qquad t = t_1, t_2, \ldots, t_n, \quad \text{Eq. 1}$$

where Y(p, t) is the signal recorded at pixel p at time t, K is the number of underlying structures, $C_k(t)$ is the kth kinetics or function and $I_k(p)$ is the spatial distribution of the corresponding structure. The purpose of FADS is to estimate the K functions (factors), $C_k(t)$ and their associated spatial distributions (factor images), $I_k(p)$, using the dixels within the dynamic images.

The present study implemented the methodology developed by Barber (*1*) and Di Paola et al. (*5*). The method generates physiological factors and factor images using the normalized TAC from each dixel. Each dixel, treated as an n-dimensional vector, is assumed to be a linear combination of the "pure" physiologic TACs. Principal component analysis of the variance of the dixels creates a new reference vector space that can be iteratively rotated until all factors and factor images are positive, (i.e., dixels have only positive contributions of the pure physiologic TACs). In summary, four steps are involved in this algorithm: (a) data preprocessing; (b) principal component analysis; (c) oblique rotation with positivity constraints; and (d) factor image computation. [For details, see Di Paola et al. (*5*)]. Two modifications in the present study are used. We found that weighting the normalized dixel vectors to scan duration improved the accuracy of the algorithm. Another modification is that we computed the coordinates of the oblique factors by minimizing the negative values in both the factors and the factor images using a constrained optimization routine (MATLAB®, MathWorks, Inc., Natick, MA). Faster convergence speeds were obtained due to this modification.

Figure 1 is the FADS flowchart we used. The original dynamic images were first masked so that only the dixels within a local region were included in the analysis. The masked images were further condensed to 8 × 8 images, resulting in 64 dixels. The image-condensing procedure improved the signal-to-noise ratio and decreased the computation time. The 64 dixels were then submitted to FADS to extract the factors as previously described. Once the factors were generated, the factor images were computed by projecting all the dixels of the original masked dynamic images onto the factors. Written in the matrix notation:

$$[Y] = [C][I], \qquad \text{Eq. 2}$$

where [Y] is the original dixels, [C] is matrix of the factor TACs and [I] is the coefficients associated with each factor, which form the factor images.

Our objective was to extract the blood TAC through the FADS. The FADS algorithm developed by Di Paola et al. (*5*), however, normalized the dixels in the data preprocessing step to give the same weight to each dixel. Since the factors obtained were in normalized units, the true magnitude of the blood curves required calculation of a scale factor. To find the scale factor, we used the highest coefficients in the blood factor images, which was usually near the center of the blood pool. Due to the noise in the PET images, we could not simply pick the highest coefficient to represent the scale factor. From a histogram of the factor coefficients, we used the average value of those coefficients that were above a certain threshold (e.g., ^{13}N-ammonia studies: 90%; FDG studies:

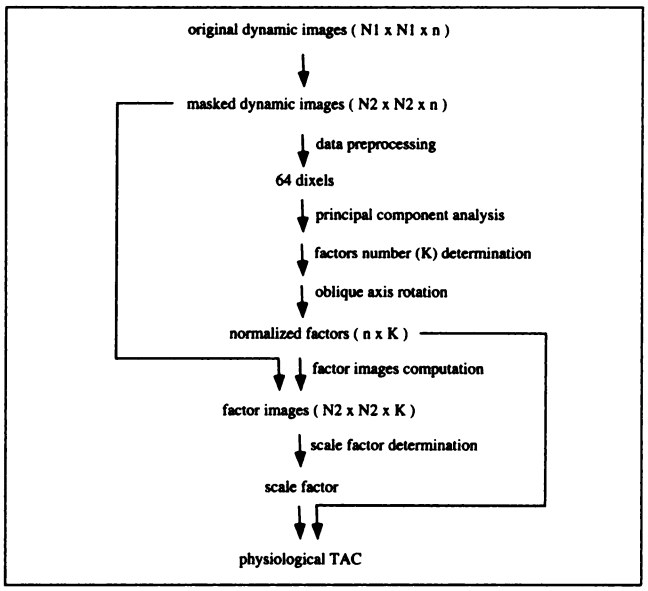

FIGURE 1. Flow chart of the FADS algorithm.

80% of the maximum) as the scale factor. The scale factor was then calculated by averaging these coefficients. Once this scale factor was obtained, the true blood TACs were calculated by multiplying the normalized blood factor by this scale factor. The sensitivity of threshold values on the scale factors was evaluated by using different thresholds (80%, 85%, 90% and 95%, respectively) in the canine studies. The results showed that the scale factors were not sensitive to the threshold values (%difference < 0.5%) if the threshold value was within the range of 80%–90%.

Computer Simulations

Three dynamic phantom images (32 × 32 × 18) were simulated individually from three structural images (factor images, Fig. 2a) and three corresponding TACs (factors, Fig. 3a). Factor 1 was a real plasma TAC following a bolus intravenous injection of FDG. Factors 2 and 3 (each contained 18 data points) were simulated from the three-compartment FDG model using the average liver and tumor tissue rate constants obtained from a melanoma study conducted in our laboratory (Table 1). Factor 1 was used as the input function. Two intensity levels (coefficients = 4, 8) in factor image 1 and eight intensity levels (coefficients = 1, 2, . . . , 8) in factor images 2 and 3 were created to simulate the spatial distributions of their corresponding factors in the images. After three dynamic images were generated and combined, Poisson noise was added (7% ~ 25% on the regions of highest image intensity). FADS was then applied to the noise-added dynamic images (Fig. 2b) to evaluate the performance of the algorithm.

Canine Nitrogen-13-Ammonia PET Studies

Ten ^{13}N-ammonia PET studies performed in four mongrel dogs (weighing 25–32.5 kg; three baseline, five dipyridamole-induced hyperemia, and two coronary occlusion) were included. Animal instrumentation and experimental procedures for the dog studies have been described in detail by Kuhle et al. (*7*). Following intravenous injection of ^{13}N-ammonia (20 mCi in 2–8 ml saline), dynamic images were obtained with a PET scanner. The dynamic sequence consisted of twelve 10-sec and six 20-sec scans for a total scan time of 4 min. The blood samples from abdominal aorta were taken at 10-sec intervals for the first 2 min. In addition, four blood samples were taken at 40, 80, 120 and 180 sec to determine the nonammonia

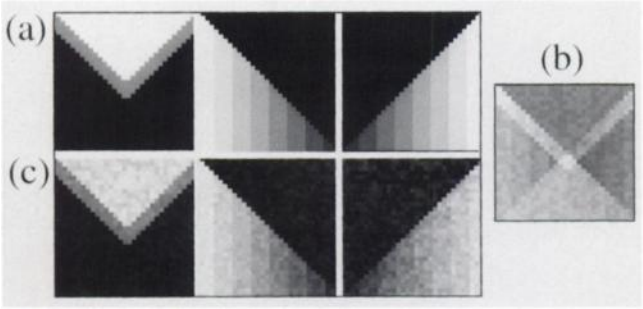

FIGURE 2. (a) Three noise-free structure images [left to right: structure I: upper triangle (two intensity levels); structure II: left white triange (eight intensity levels); structure III: right white triangle (eight intensity levels)] were used to simulate the dynamic phantom images (32 × 32 × 18 matrix). (b) The Poisson-noise added composite image was obtained by adding the three individual dynamic images (frame 14). (c) Three FADS-generated factor images obtained from noise-added composite phantom images of (b) are similar to the original images in (a).

metabolites in the arterial input function. Assays of ^{13}N plasma concentrations were performed in a well counter after centrifugation of the blood samples. Each blood TAC was corrected for physical decay and nonammonia metabolites. The percentages of nonammonia metabolites in the blood at the in-between times were derived by linear interpolation of metabolites determined from the four arterial samples. A cylinder phantom filled with $^{68}Ge/^{68}Ga$ solution was scanned on the same day of the PET study to determine the conversion factor between image data in units of counts/min/pixel and well counter data in units of count/min/ml.

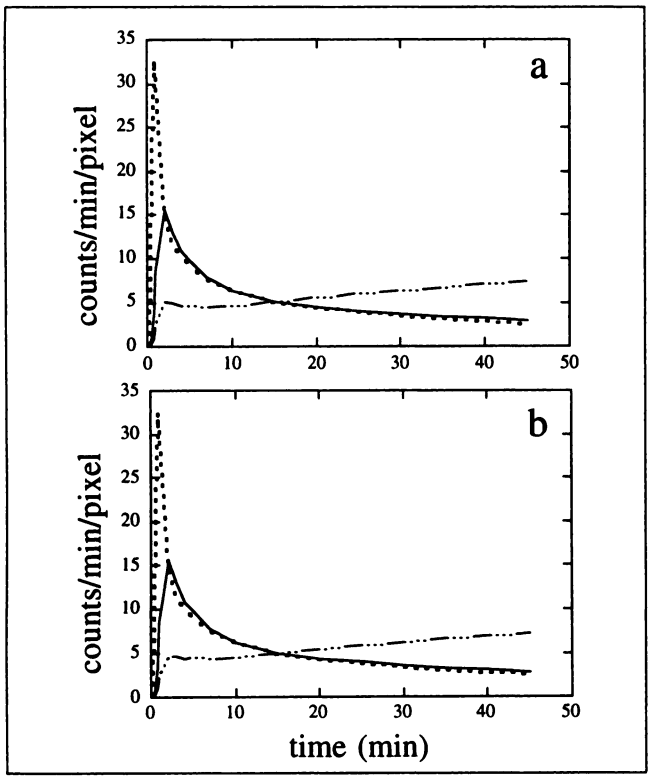

FIGURE 3. (a) Three noise-free TACs [corresponding to structure I (dotted line), structure II (line with dots) and structure III (solid line)] used to simulate the dynamic phantom images of Figure 2. (b) Three corresponding FADS-generated factors obtained from Poisson-noise added composite phantom images from FADS are similar to the original TACs.

The 128 × 128 transaxial images (1.38 mm^2/pixel) were reconstructed using a Shepp-Logan filter with a cutoff frequency of 0.48 Nyquist frequency, yielding an in-plane spatial resolution of ~10.5 mm FWHM. Fifteen simultaneous cross-sectional images, with 6.75 mm plane separation (center-to-center), were generated with a total axial field of view of 10.8 cm. Photon attenuation was corrected with a 20-min transmission scan using a $^{68}Ge/^{68}Ga$ external ring source. The 15 contiguous transaxial images of each study were then reoriented into six left ventricular short-axis slices as described previously (*8*).

The 128 × 128 × 18 short-axis dynamic images (midventricular plane, either plane 2 or 3 of the six contiguous short-axis images in each study) were first masked to form a 64 × 64 × 18 dynamic image file. The masked area included the right, left ventricular blood pools and entire myocardium. The masked images were then submitted to the FADS (Fig. 1). The first three factors were extracted. The three 64 × 64 factor images were then computed by projecting all dixels of the original masked 64 × 64 dynamic images onto the three factors.

Human FDG-PET Studies

Following intravenous injection of 10 mCi FDG, dynamic images were obtained with the PET scanner which simultaneously acquired 15 image planes, each 6.75 mm in a 10.8-cm axial field of view. The dynamic sequence in the cardiac FDG-PET study consisted of nine 10-sec, two 30-sec, three 5-min and five 10-min scans for a total scan time of 67.5 min. The breast cancer FDG-PET study was performed over the superior part of the liver (plane 1 contained the blood pool). The dynamic sequence consisted of twelve 10-sec, four 30-sec, and fourteen 4-min scans for a total scan time of 60 min. In both studies, photon attenuation was corrected with 20-min transmission scans using a $^{68}Ge/^{68}Ga$ external ring source. The 128 × 128 transaxial images were reconstructed using a Shepp-Logan filter with a cutoff frequency of 0.30 Nyquist, yielding an in-plane spatial resolution of ~10 mm FWHM. The masked transaxial images [cardiac study: 64 × 64 matrix (2.45 mm^2/pixel); breast cancer study: 32 × 32 matrix (4.99 mm^2/pixel)] at the level of heart were then submitted to FADS. The first three factors, which account for ~80% of the total variance in the data, were extracted. The blood samples were taken from a hand vein, heated to 44°C to arterialize the blood, at 5–10-sec intervals over the first 3 min and at progressively lengthening intervals for the remaining duration of the study. Conversion of ^{18}F plasma concentrations from well counter counts to image data was the same as described in the ^{13}N-ammonia studies.

Validation of FADS Blood Factors

To validate the replacement of blood sampling with the FADS-generated blood factor, we compared the blood factors with aortic plasma TACs and ROI-generated left ventricular TACs. Since the ROI method was sensitive to the location and size of the ROIs, we used small ROIs (~30–60 mm^2) located at the center of left ventricular cavities to generate the left ventricular TACs that avoided myocardial spillover activities. The blood TACs from the different methods were then integrated from 0 to 2 and 0 to 3 min. The ratios between different integrals were compared. The accuracy of blood factors was also evaluated by using the different blood TACs as the input functions to the model fittings to estimate the myocardial blood flow (MBF in milliliter per minute per gram) and glucose metabolic rates. The two-compartment model established by Smith et al. was used in estimating regional MBF (*9*).

TABLE 1
Rate Constants Used to Simulate the Factor Curves in Phantom Simulations

Factor	Tissue	Rate constants† K_1^* (ml/min/g)	k_2^* (min^{-1})	k_3^* (min^{-1})	k_4^* (min^{-1})
2‡	Tumor	0.243	0.780	0.101	0
3‡	Liver	0.864	0.981	0.005	0.016

†Unpublished data from our laboratory. Tumor: mean values from 25 melanoma studies; liver: mean values from 10 volunteers.
‡Eighteen data points were simulated in each factor curve with midscan times at T = 0.1, 0.3, 0.6, 0.9, 1.5, 2.5, 3.5, 4.5, 6, 8.5, 12.5, 17.5, 22.5, 27.5, 37.5, 42.5 and 47.5 min.

The three-compartment FDG model developed by Phelps et al. was used to compare the microparameters (K_1^*, k_2^*, k_3^*, k_4^*) and macroparameter (Knlr) of glucose metabolism. A blood volume term was also included in the model (*10,11*). In the myocardial MBF and glucose metabolic rate analysis, each myocardial section was divided into eight sectors, which were equally divided (45° for each sector). The sectorial ROIs were defined by the two contours separated radially by three pixels and centered at the peak of myocardial circumferential activity (*7*). Eight sectorial TACs were then generated and corrected for partial volume effect (*7*). In the breast cancer study, the TAC of liver metastases was used.

RESULTS

Computer Simulation

Figures 2c and 3b show the three factor images and three factors generated from FADS when the noise-added composite phantom images of the highest simulated noise level (~25%) were used. Except for noise, each factor image showed excellent separation and resembled the original corresponding structural image (Fig. 2a). The shapes of the three factors were almost identical to the original TACs (Fig. 3). Figure 4 shows the point-to-point percent differences between the original TACs and FADS-generated factors. Overall, the percent differences between the two sets of curves were small (~2%). Note that the larger percent differences corresponded to small TAC values, and the magnitudes of the differences in these areas are actually extremely small. For the simulations with lower noise levels (<25%), the differences between the original TACs and the FADS-generated factors were even smaller.

Canine Nitrogen-13-Ammonia PET Studies

Three factor images and their corresponding factors were identified as right ventricular, left ventricular blood pools, and myocardial activities in a canine ^{13}N-ammonia PET study (Fig. 5, 6a). The three factors accounted for ~95% of the total variance in the data. The results were consistent in the ten canine studies. Three factors were similar to the TACs generated from ROI drawings upon three structures (right ventricular: ~170 mm^2; left ventricular: ~390 mm^2, myocardium: ~20 mm^2) in the original dynamic images (Fig. 6b). Figure 7 shows the nonammonia

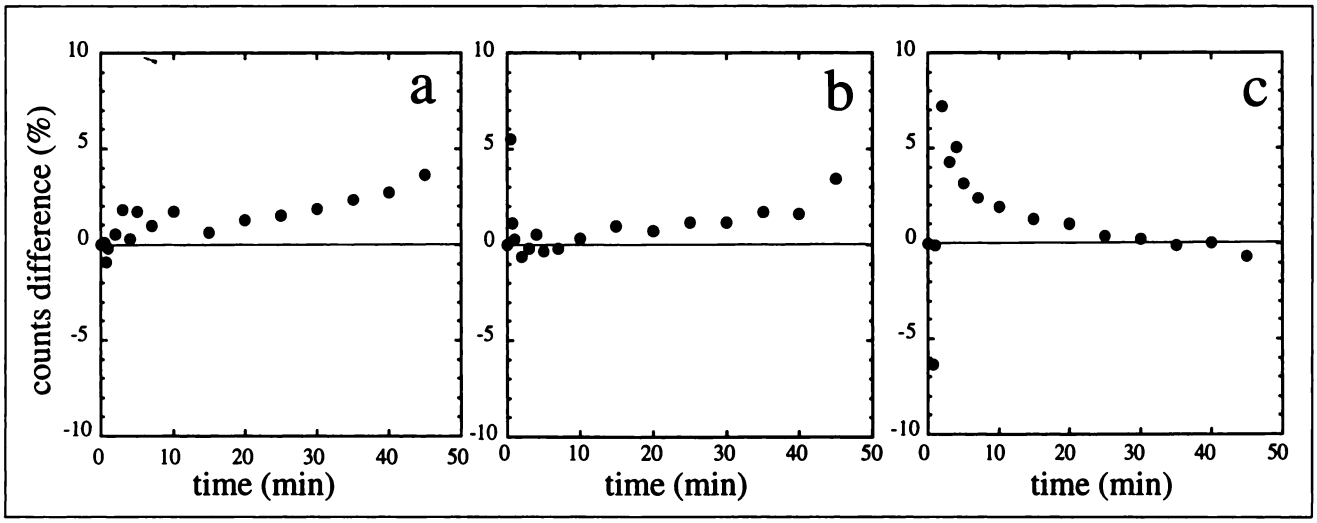

FIGURE 4. Point-to-point percent differences between FADS-generated (a) factor 1, (b) factor 2 and (c) factor 3 and the corresponding noise-free TACs, which were used to generate the composite phantom images. The larger percent differences correspond to small TAC values.

FIGURE 5. Three factor images obtained from a canine ^{13}N-ammonia PET dynamic study using FADS. The three structures were identified as: (left) right ventricular, (middle) left ventricular blood pools and (right) myocardium.

metabolite-corrected plasma samples, ROI (~30 mm^2) generated left ventricular TAC and the scale-corrected left ventricular factor from a dog study. Except for a time lag of the plasma samples, the overall shapes of the plasma samples and left ventricular factor were similar. The time lag of plasma samples might be due to the transit time of radioactive bolus from the left ventricular cavity to the sampling site in the abdominal aorta. Compared with the left ventricular TACs from the conventional ROI method, most of the factor curves were less noisy. Table 2 summarizes the ratios of integrals between the different blood TACs. The results demonstrated that there were no statistically significant differences between the integrals of the left ventricular factors and plasma samples (or left ventricular TACs).

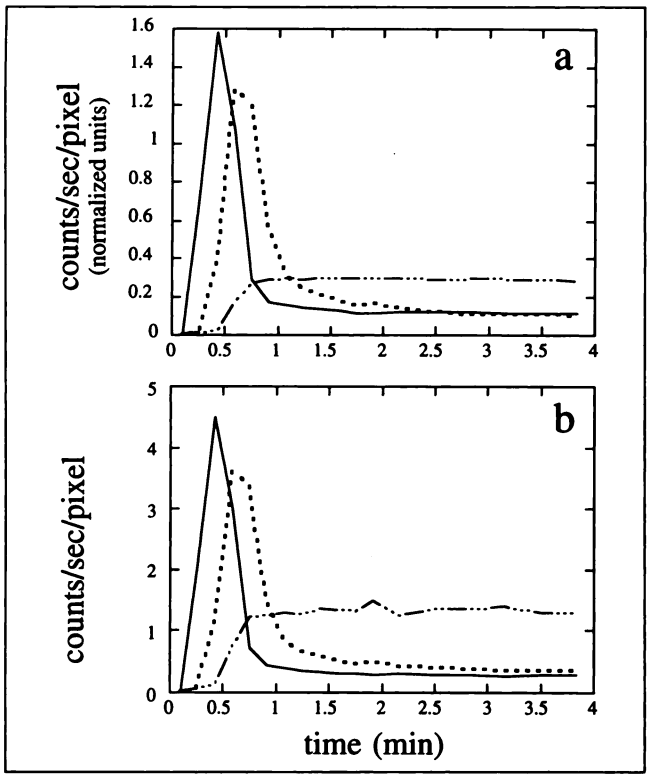

FIGURE 6. (a) Three FADS-generated factors from a canine ^{13}N-ammonia PET dynamic study. Each factor corresponded to right ventricular (solid line), left ventricular (dotted line) blood pools or myocardial structure (line with dots). (b) ROI-generated TACs from the original dynamic images of the same dog study [right ventricular (solid line), left ventricular (dotted line), and myocardium (line with dots)].

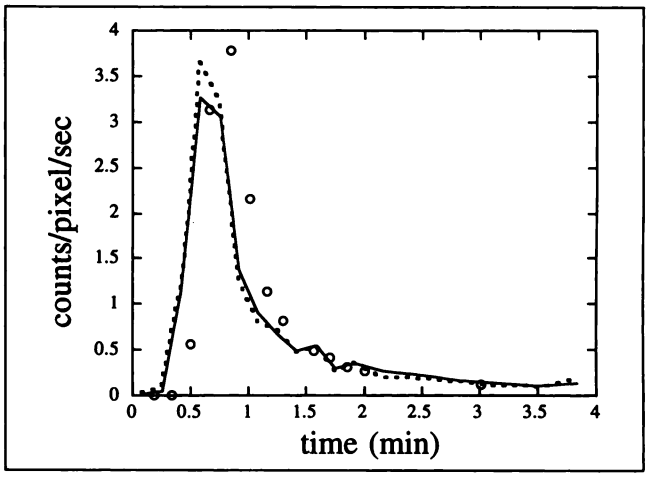

FIGURE 7. Nonammonia metabolites-corrected TAC from plasma samples (open circles), ROI-generated left ventricular TAC (dotted line) and scale-corrected left ventricular factor (solid line) of a canine ^{13}N-ammonia PET study.

In the two-compartment model fittings, MBFs obtained from the left ventricular factors as the input function correlated well with those obtained from plasma samples as the input function (Fig. 8a, $y = 1.01x + 0.16$; $r = 0.99$; $n = 80$). The MBFs obtained with the left ventricular factor as the input function also showed good correlation with those obtained from conventional left ventricular TACs as the input function (Fig. 8b), $y = 1.06x - 0.04$; $r = 1.00$; $n = 80$).

Human FDG-PET Studies

In FDG-PET cardiac studies, right ventricular and left ventricular blood pools could not be separated and appeared in the same factor image (Fig. 9). The single blood factor, however, was similar to the plasma samples (Fig. 10a). Furthermore, the spillover activity in the conventional ROI-generated left ventricular TAC was not observed in the blood factor. By applying the blood factor to the three-compartment FDG model to estimate the myocardial glucose metabolic rate, the macroparameter, Knlr, which is proportional to the glucose metabolic rate, correlated well with those obtained by using the plasma curve as

TABLE 2
Integral Ratios of Different Blood TACs from Ten Canine Studies

Integrating time	No.	Mean ± s.d. ratio	
		Factor/Plasma	Factor/LV TAC
0–2 min	10	1.00 ± 0.07*	0.99 ± 0.05*
0–3 min	10	1.01 ± 0.06*	0.99 ± 0.04*

*The ratio is nonsignificantly different from 1.00 at the p = 0.05 level of confidence. LV = left ventricular.

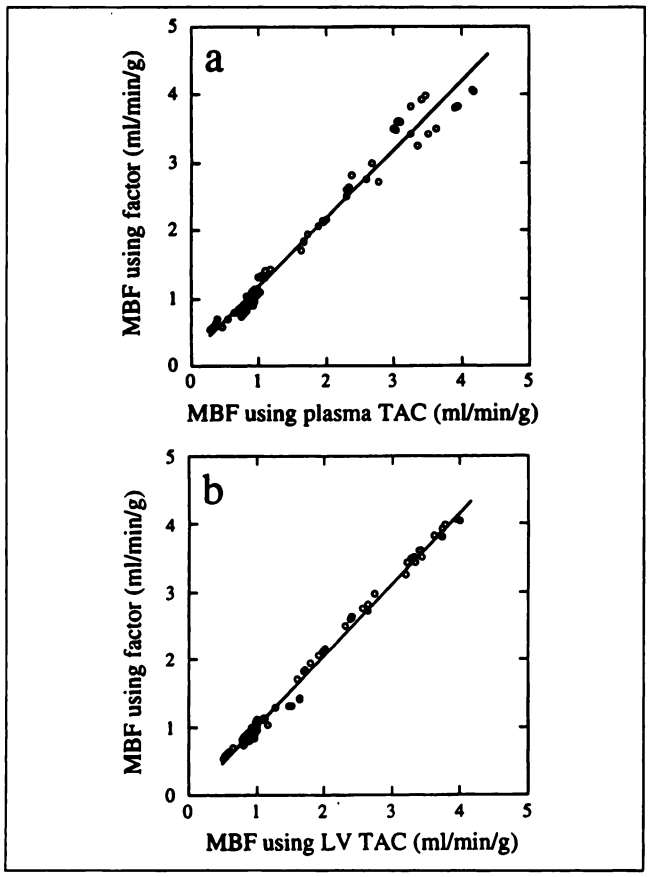

FIGURE 8. (a) Correlation of MBFs obtained using the blood factors and those plasma samples as the input functions ($y = 1.01x + 0.16$; $r = 0.99$; $n = 80$). (b) Correlation of MBFs obtained using blood factors and conventional left ventricular TACs as the input functions ($y = 1.06x - 0.04$; $r = 1.00$; $n = 80$).

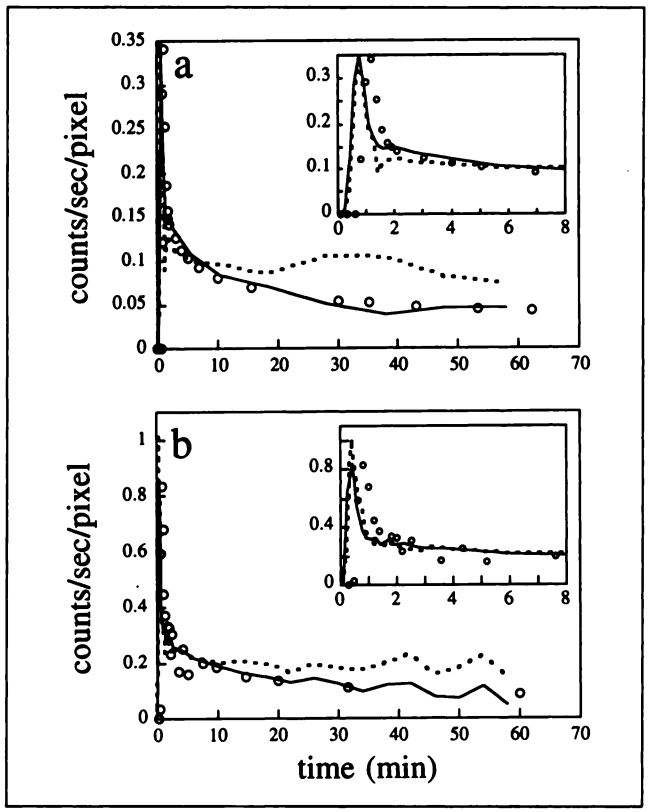

FIGURE 10. Plasma samples (open circles), ROI-generated left ventricular TAC (dotted line) and FADS-generated blood factor (solid line) from (a) cardiac and (b) breast cancer FDG-PET dynamic studies. Scales of the first 8 min of data were expanded and shown in the small insets.

the input function (Fig. 11a, $y = 0.98x + 0$; $r = 1.0$; $n = 8$). If, however, the ROI-generated (~60 mm^2) left ventricular TAC was used as the input function without spillover correction, the correlation was worse. The estimated Knlr using an ROI-generated (~60 mm^2) left ventricular TAC was not reliable (Fig. 11b, $y = 0.58x + 0$; $r = 0.94$; $n = 8$).

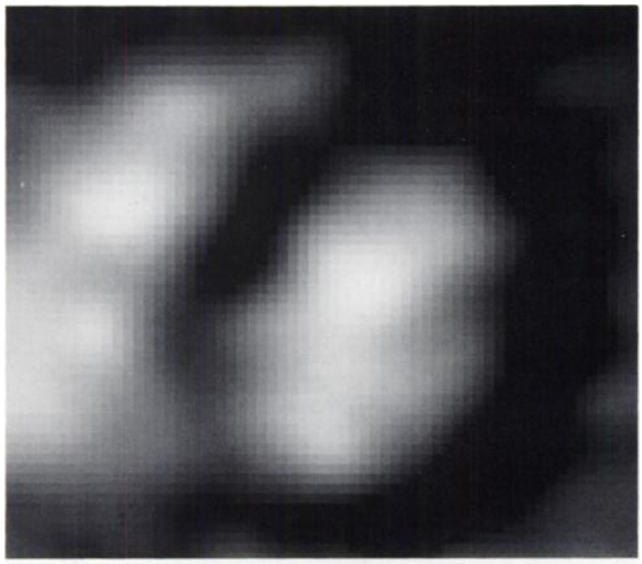

FIGURE 9. Blood factor image obtained form a cardiac FDG-PET dynamic study using FADS.

Figure 10b shows the plasma samples, the ROI-generated left ventricular TAC and FADS blood factor from a FDG-PET study of a patient with breast cancer. Even with a small ROI (~60 mm^2) located at the center of the blood pool, the left ventricular curve obtained was noisy and had a large amount of spillover from myocardial activity. Although noisy, the blood factor was similar to the plasma TAC. Compared to canine ^{13}N-ammonia left ventricular TACs, human FDG left ventricular TACs contained more spillover activities from the myocardium to left ventricular blood pools. This might be due to patient movement and the transaxial images used in the FDG studies. Table 3 summarizes the microparameters and macroparameters obtained by applying the different blood curves to the three-compartment FDG model to estimate lesion glucose metabolic rates. As found with the cardiac studies, the microparameters and macroparameters were similar when the plasma and factor methods were used. The parameter results obtained from the ROI-generated left ventricular curve were not reliable. Even with the conventional method (*13*) to correct for the spillover activity, the results still contained large errors when compared with those us-

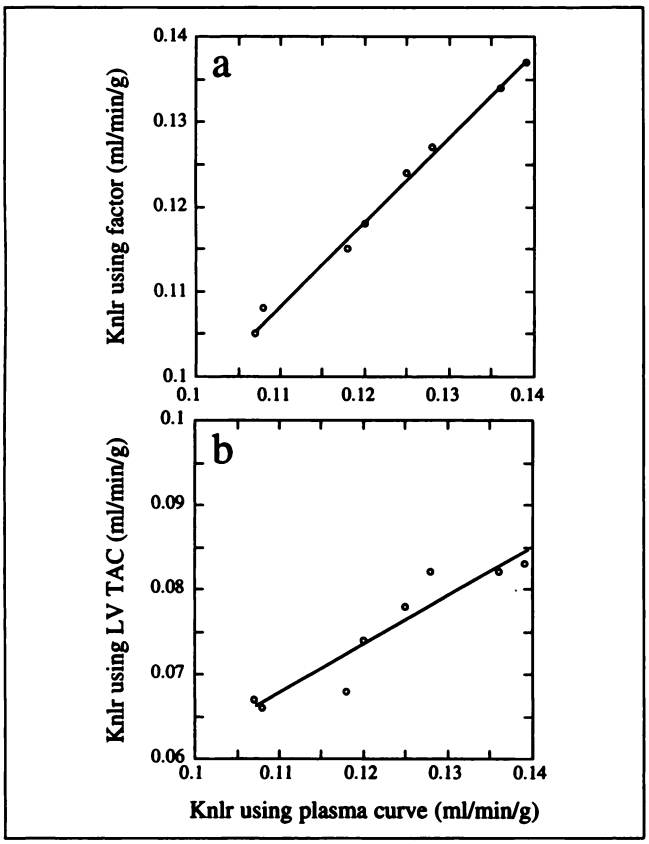

FIGURE 11. (a) Correlation of macroparameters (Knlr) obtained using blood factors and plasma samples as the input functions (y = 0.98x + 0; r = 1.00; n = 8). (b) Correlation of macroparameters (Knlr) obtained using conventional left ventricular TACs and plasma samples as the input functions (y = 0.58x + 0; r = 0.94; n = 8). Knlrs were estimated from the TACs of eight equally divided sectorial ROIs (45° for each sector) in a patient's myocardial section.

ing the plasma curve (i.e., between row 1 and row 4 of Table 3).

DISCUSSION

The use of factor analysis in nuclear medicine has been reported in the literature for more than 20 yr (*1–4*). One of the goals behind many of these works was the desire to eliminate ROI analysis (*12*). Two major considerations prevented general acceptance of this technique. The first consideration was the difficulty in interpreting the factors. The most powerful form of factor analysis, in terms of the efficiency with which data can be reduced in volume, is principal components analysis (PCA). Based on orthogonal transforms, PCA produced factors that could not be related directly to physiological TACs in the data. It was recognized that physiologically meaningful factors cannot have elements of negative values. FADS extended PCA and was followed by techniques of oblique rotations with the positivity constraints, which produced factors closer to the true physiological factors than PCA. The factors may still not, however, represent the true physiological TACs if the pure component TACs do not exist in the original data (e.g., a tissue activity superimposed on a background activity). Both the planar and axial resolutions of nuclear medicine imaging devices have limited the accuracy of FADS to extract pure TACs. Another negative aspect of FADS was the computation burden encountered when oblique rotations were required to compute the factors.

Functional imaging with PET in numerous applications generates images with biochemical or physiological information as well as improved resolution compared to conventional nuclear medicine scintigraphy. The quantitation of physiological parameters by PET imaging, however, has been complicated by several factors: (a) the invasiveness of arterial blood sampling in humans to obtain the blood TACs and (b) the limited spatial resolution of PET scanners, which results in spillover and partial volume effects. To avoid invasive blood sampling, left ventricular TAC from user-drawn ROIs have been used previously. The left ventricular curve has been corrected for spillover from myocardial tissue to the left ventricle by using the spillover fraction from the myocardium to blood [calculated as the difference in activity between the arterial and left ventricular curve at the last sampled point divided by the average activity at this time in the whole myocardium (*13*)]. The spillover of radioactivity from the blood pool to the tissue at early times, and the spillover from the tissue to the blood pool at later times, complicates the blood and tissue TACs obtained from the PET images and affects the accuracy of the spillover correction. The results in Table 3 show that the left ventricular TAC without spillover correction was almost useless in the FDG studies. Even using the left

TABLE 3
Microparameters and Macroparameters Obtained from Three-Compartment Model Fitting Using Different Input Functions in a Breast Cancer FDG-PET Study

Input function	Rate constants				Knlr
	K_1^* (ml/min/g)	k_2^* (min^{-1})	k_3^* (min^{-1})	k_4^* (min^{-1})	(ml/min/g)
Plasma samples	0.43	0.71	0.02	0.00	0.0102
FADS blood factor	0.61	0.90	0.02	0.00	0.0107
LV curve (no correction)	0.55	0.72	1.00e-08	0.92	1.00e-08
LV curve† (with correction)	0.67	0.86	0.03	0.01	0.0212

†The left ventricular (LV) TAC was corrected using the conventional spillover correction method (*13*).

ventricular TAC with the spillover correction, the microparameters and macroparameter obtained from three-compartment model fitting were still not comparable to those obtained using the plasma samples as the input function. Although a more complicated procedure can be used which corrects left ventricular TACs for spillover activities based on geometric physical correction (*14*), a simple but reliable procedure to extract the pure blood curve is advantageous.

In the present study, we have validated the usefulness of FADS-generated blood factors in both canine ^{13}N-ammonia studies and human FDG-PET studies. The results in Figures 7 and 10 show that FADS with positivity constraints was sufficient to extract blood TACs comparable to the plasma samples in both studies. Furthermore, the MBF and glucose metabolic index (Knlr) estimated from using FADS-generated blood factors correlated well with those estimated from using plasma samples (Figs. 8, 11 and Table 3). PET imaging with ^{13}N-ammonia and FDG has been shown to be useful for identifying myocardial ischemia and defining tissue viability in patients with ischemic heart disease (*15,16*). The feasibility of extracting the pure blood TAC from FADS provides a simple, noninvasive approach to determine the input function for these studies. The breast cancer FDG-PET study demonstrated that the noninvasive "pure" blood TAC can be extracted from the same dynamic study if the patient's ventricular cavity is in the field of view.

As shown in Figure 9, the right ventricular and left ventricular activities could not be separated by FADS in FDG-PET studies. This might due to the 60-min total scan time and the difference of only ~10 sec in peak activities of right ventricular and left ventricular TACs. The present scan protocol (as described earlier) did not allow us to separate the right ventricular and left ventricular TACs in the FDG images. The FADS blood factors, however, resembled the plasma TACs and provided accurate parameter estimations.

In this study, the feasibility of extracting the "pure" arterial TACs from human adult dynamic FDG-PET images using FADS was demonstrated. The separation of the "pure" arterial TAC in a small monkey or pediatric dynamic PET study using FADS, however, was found to be unsuccessful due to the small size of the cardiac chamber that causes extensive mixture of TACs of different structures. The errors arose from the assumption that dixels with no activity contribution from other structures ("pure" dixels) existed. Therefore, the resampling in the data preprocessing step is crucial. Coarse sampling relative to image resolution may affect the accuracy of the FADS blood factor. In this study, each dixel area in the canine ^{13}N-ammonia, human FDG cardiac and FDG breast cancer studies are 88, 157 and 80 mm^2, respectively.

The programs used in the present study were implemented in a SPARC® (Mountain View, CA) 10 SUN workstation. Except for the manually applied mask, all the other steps could be automated (Fig. 1). For a three-factor study, the entire FADS procedure required approximately 2–5 min computation time. The major time-consuming step was axis oblique rotation. Because the present study used a command language (MATLAB®), the computation time is expected to shorten by implementing the programs using a lower level language such as C.

A factor that may affect the accuracy of blood TAC extraction is noise in the original dynamic images. The phantom simulation studies (three different noise levels, ~7%–25%) demonstrated that the factors generated from FADS were not affected by the different noise levels added to the dynamic images. Since the objective of this study was to extract the blood TAC, we did not try to account for the noise in the factor images.

CONCLUSION

FADS with the positivity constraints, as demonstrated in this study, has the ability to accurately extract the "pure" blood TAC directly from dynamic PET images. Ultimately, the method may allow reliable quantitation of biological information from PET studies without requiring blood sampling, ROI drawing and spillover correction.

ACKNOWLEDGMENTS

The authors thank the UCLA cyclotron staff for synthesizing the ^{13}N-ammonia and FDG compounds used in this study; Mr. Ron Sumida and the UCLA PET scanner staff for performing the PET studies; and Drs. E.J. Hoffman, M. Dahlbom, A.R. Ricci, K. Gardner and D. Truong for instrumentation, computer hardware and software support. This work was supported in part by National Institutes of Health grant K08 CA 01669-02.

REFERENCES

1. Barber DC. The use of principal components in the quantitative analysis of gamma camera dynamic studies. *Phys Med Biol* 1980;25:283–292.
2. Cavailloles F, Bazin JP, Di Paola R. Factor analysis in gated cardiac studies. *J Nucl Med* 1984;25:1067–1079.
3. Samal M, Surova H, Karny M, Marikova E, Michalova K, Dienstbier Z. Enhancement of physiological factors in factor analysis of dynamic studies. *Eur J Nucl Med* 1986;12:280–283.
4. Helal BO, Frouin F, Schaison G, et al. Diagnosis of malignancy in thyroid nodules by factor analysis of spectral and dynamic structures: a simultaneous dual-isotope dynamic study with thallium-201 and iodine-131. *Eur J Nucl Med* 1992;19:517–521.
5. Di Paola R, Bazin JP, Aubry F, et al. Handling of dynamic sequences in nuclear medicine. *IEEE Trans Nucl Sci* 1982;NS29:1310–1321.
6. Frouin F, Bazin JP, Di Paola M, Jolivet O, Di Paola R. FAMIS: a software package for functional feature extraction from biomedical multidimensional images. *Comput Med Imaging Graph* 1992;16:81–91.
7. Kuhle WG, Porenta G, Huang SC, et al. Quantification of regional myocardial blood flow using ^{13}N-ammonia and reoriented dynamic positron emission tomographic imaging. *Circulation* 1992;86:1004–1017.
8. Kuhle WG, Porenta G, Huang SC, Phelps ME, Schelbert HR. Issue in the quantitation of reoriented cardiac PET images. *J Nucl Med* 1992;33:1235–1242.
9. Smith GT, Huang SC, Nienaber CA, Krivokapich J, Schelbert HR. Noninvasive quantification of regional myocardial blood flow with N-13 ammonia and dynamic PET [Abstract]. *J Nucl Med* 1988;29:940.
10. Phelps ME, Huang SC, Hoffman EJ, Selin CJ, Sokoloff L, Kuhl DE. Tomographic measurement of local cerebral glucose metabolic rate in humans with (F-18) 2-fluoro-2-deoxy-D-glucose: validation of method. *Ann Neurol* 1979;6:371–388.
11. Hawkins RA, Phelps ME, Huang SC. Effects of temporal sampling, glucose metabolic rates, and disruptions of the blood-brain barrier on the FDG model with and without a vascular compartment: studies in human brain tumors with PET. *J Cereb Blood Flow Metab* 1986;6:170–183.

12. Barber D, Martel A. Factor analysis revisited. *Eur J Nucl Med* 1992;19: 467–468.
13. Gambhir SS, Schwaiger M, Huang SC, et al. Simple noninvasive quantification method for measuring myocardial glucose utilization in humans employing positron emission tomography and fluorine-18-deoxyglucose. *J Nucl Med* 1989;30:359–366.
14. Henze E, Huang SC, Rabit O, et al. Measurements of regional tissue and blood-pool radiotracer concentrations from serial tomographic images of the heart. *J Nucl Med* 1983;24:987–996.
15. Marshall RC, Tillisch JH, Phelps ME, et al. Identification and differentiation of resting myocardial ischemia and infarction in man with positron computed tomography, ^{18}F-labeled fluorodeoxyglucose and N-13 ammonia. *Circulation* 1983;67:766–777.
16. Brunken R, Tillisch J, Schwaiger M, et al. Regional perfusion, glucose metabolism and wall motion in chronic electrocardiographic Q-wave infractions. Evidence for persistence of viable tissue in some infarct regions by positron emission tomography. *Circulation* 1986;73:951–963.

(continued from page 1560)

FIRST IMPRESSIONS:

FOCAL INTRA-ABDOMINAL INDIUM-111-LEUKOCYTE ACCUMULATION: IS IT ALWAYS AN ABSCESS?

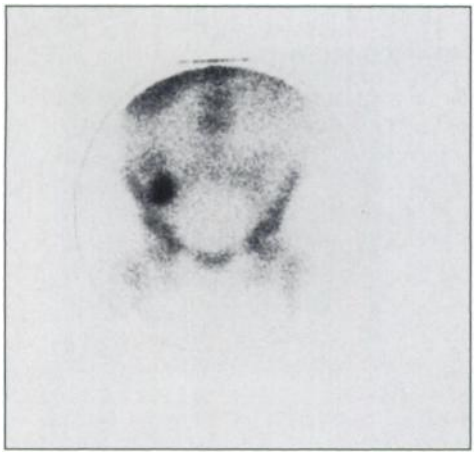

FIGURE 1.

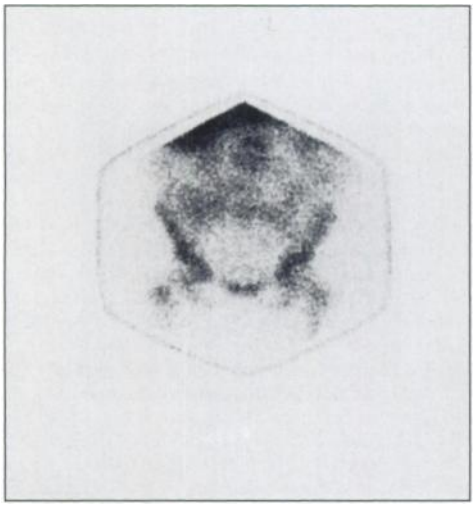

FIGURE 2.

PURPOSE

A 45-yr-old woman with acute liver failure secondary to acetominophen overdose underwent ^{111}In-leukocyte scintigraphy because of persistent fever. Twenty-four hour delayed spot images of the entire body revealed intense, focal ^{111}In-leukocyte accumulation only in the lower right abdominal quadrant (Fig. 1) that was typical of abscess formation. Because abdominopelvic CT obtained 3 days earlier revealed no abnormality in this area, repeat imaging was performed 24 hr later and showed dispersal of labeled leukocytes throughout the colon (Fig. 2). This changing scintigraphic pattern was most consistent with localized ileocecal colitis rather than abscess formation. Colonoscopy 2 days later confirmed focal cecal inflammation and several large ulcers. This case illustrates two points: correlating the scintigraphic findings with current anatomic imaging modalities and the value of selective repeat, delayed imaging to avoid misdiagnosis of abscess formation.

TRACER

Autologus mixed leukocytes labeled with 0.5 mCi (18 MBq) ^{111}In-oxine

ROUTE OF ADMINISTRATION

Intravenous

TIME AFTER INJECTION

24 and 48 hours

INSTRUMENTATION

Large field of view Siemens Basicam with a medium-energy collimator

CONTRIBUTOR

Dwight M. Achong, New England Medical Center, Boston, MA